Li + Diffusion and Its Structural Basis in the Nanocrystalline and Amorphous Forms of Two-Dimensionally Ion-Conducting Li x TiS 2

ARTICLE *in* THE JOURNAL OF PHYSICAL CHEMISTRY B · JULY 2001

Impact Factor: 3.3 · DOI: 10.1021/jp011200f · Source: OAI

2 AUTHORS, INCLUDING:

Paul Heitjans
Leibniz Universität Hannover
265 PUBLICATIONS **3,613** CITATIONS

Li^+ Diffusion and Its Structural Basis in the Nanocrystalline and Amorphous Forms of Two-Dimensionally Ion-Conducting Li_xTiS_2

Rudolf Winter[†] and Paul Heitjans*

Institut für Physikalische Chemie und Elektrochemie, Universität Hannover, 30167 Hannover, Germany

Received: March 29, 2001

The layered fast ion conductor Li_xTiS_2 ($x \approx {}^2/_3$) has been prepared in nanocrystalline (n-Li_xTiS_2) and amorphous (a-Li_xTiS_2) forms. Hence, a direct comparison of the lithium diffusion in a homogeneously and a heterogeneously disordered material with the same composition is possible. As a reference system, polycrystalline Li_xTiS_2 (in its hexagonal modification, h-Li_xTiS_2) was also investigated by measuring the temperature and frequency dependencies of the spin−lattice relaxation rate T_1^{-1} of ^{7}Li. The activation energies for individually jumping ions as obtained from the low-temperature flanks of the rate maxima are 190, 160, and 70 meV in h-,n-, and a-Li_xTiS_2, respectively. The frequency dependence of T_1 is sublinear for both disordered forms, which is explained in terms of the unified site relaxation model. ^{7}Li nuclear magnetic resonance (NMR) spectra of n-Li_xTiS_2 tend, contrary to those of h-Li_xTiS_2 and a-Li_xTiS_2, to decompose into broad and narrow central line components. The relative intensity of the narrow component, which is attributed to fast moving Li ions in the interfacial regions, is temperature dependent and reaches 50% at 360 K. A schematic model for the ionic conduction process in two-dimensional nanocrystalline fast ionic conductors is proposed, introducing grain surface pathways as the dominant track for mobile ions.

Introduction

Li_xTiS_2 is a well-known prototype cathode material for high-energy density batteries. Its fundamental electrochemical properties have been studied for more than 20 years.[1] From the more technological point of view, despite its economic and ecological limitations, Li_xTiS_2 is among the materials currently considered for the development of all solid-state batteries.[2] Its advantages as a cathode material are its stability in the entire intercalation range $0 \leq x \leq 1$ and the highly reversible insertion reaction with reasonable free enthalpy. Thus, cells on the basis of Li_xTiS_2 can be cycled many times without running into problems regarding the structure of the material. It is therefore used in modern rocking-chair battery prototypes.[3,4]

Materials in a disordered state often show markedly improved diffusivity as compared to their coarse-grained or single-crystalline counterparts. This is a common observation for homogeneously disordered, that is, amorphous,[5,6,7] as well as heterogeneously disordered, for example, nanocrystalline,[7,8] materials. In both cases, the detailed structure representing the dominant kind of disorder is strongly dependent on the preparation process. Thus, for disordered materials, the history of the samples has to be taken into account when interpreting measured data. In this study, an amorphous sample ("a-Li_xTiS_2") was obtained via an organometallic synthesis route, while a set of nanocrystalline samples ("n-Li_xTiS_2") was prepared by ball-milling of the polycrystalline material. In both cases, lithium insertion was achieved chemically by reaction with *n*-butyllithium. This technique is easier to handle than and was confirmed to be chemically equivalent to the electrochemical procedure.[9]

To investigate the effects of the order state in Li_xTiS_2, samples of amorphous, nanocrystalline, and polycrystalline Li_xTiS_2 were investigated. As a coarse-grained reference system, the polycrystalline hexagonal modification ("h-Li_xTiS_2") was used, which is a fast two-dimensional lithium ion conductor[1] and, being semimetallic, also a reasonable electronic conductor.[10] A comparative ^{7}Li NMR study of the mechanism and dimensionality of lithium motion in the hexagonal (two-dimensional) and cubic (three-dimensional) modifications of Li_xTiS_2 has been conducted earlier in this group.[11]

Spin−lattice relaxation measurements reveal information on the diffusion properties of the material under study. Here, the temperature dependence of the relaxation rate T_1^{-1} of ^{7}Li is Arrhenius-type, and the activation energies for jumps of individual lithium ions may be calculated from the data.[7] Spin−lattice relaxation rates have also been measured as a function of frequency in order to gain information on the underlying diffusion mechanism. An analysis of the temperature-dependent line shape of the spectral lines obtained by Fourier transformation of the time-domain NMR signal is the basis for a schematic model of the structural conditions determining the diffusion mechanism in a nanocrystalline layered material. In the framework of this model, a close relationship may be derived between the diffusion processes in poly- and nanocrystalline two-dimensional ion conductors.

Experimental Section

I. Sample Preparation and Characterization. The *amorphous sample* was synthesized following an organometallic route[12] using a precursor (hexamethyldisilthiane) with large organic rests. These sterically hinder the reaction with $TiCl_4$, thereby ensuring that formation kinetics dominates growth kinetics of TiS_2 crystallization nuclei when these are precipitated

[†] Present address: Department of Physics, University of Wales, Aberystwyth, United Kingdom.

* E-mail: heitjans@mbox.pci.uni-hannover.de. Fax: +49-511-762-4009.

10.1021/jp011200f CCC: $20.00
Published on Web 06/08/2001

TABLE 1: Sample Identifiers, Milling Time, Average Particle Size L_i (As Obtained from Eq 1), and Activation Energies E_{nmr}^{lT} (as Defined in Eq 2)

sample	milling time (h)	L_i (nm)	E_{nmr}^{lT}(eV)
h		≈1000	0.19
n1/2	0.5	20	0.17
n1	1	14	0.19
n2	2	12	0.16
n50	50	12	0.12
a			0.07

from a liquid reactant mixture. Afterward, lithium ions were inserted by stirring the host material for 2 days in a solution of 1.6 M *n*-butyllithium in hexane,[13] yielding a lithium content of $x \approx 2/3$. The *nanocrystalline samples* were generated by lithium intercalation into polycrystalline TiS_2 (Aldrich), using the same intercalation procedure as with the amorphous material. The obtained polycrystalline Li_xTiS_2, after annealing at 700 K for 10 days, was milled in a SPEX 8000 high-energy ball-mill with a corundum vial set in an airtight container for 0.5−50 h (cf. Table 1).

Obviously, any technique used to prepare disordered Li_xTiS_2 samples will involve two steps: the insertion of lithium ions and the establishment of the desired order state. In principle, the sequence of the two steps is arbitrary, but because a homogeneous distribution of lithium ions is desirable, an annealing step should be added after the insertion whenever possible. The procedure leading to the amorphous material does not allow an intermediate thermal treatment. Therefore, to examine the additional effect of diffusion in a chemical potential gradient instead of the pure self-diffusion which is under study here, one nanocrystalline sample was prepared by the inverted sequence "ball-milling−intercalation".

X-ray diffractograms of all samples were taken in order to estimate the particle diameter of n-Li_xTiS_2 (cf. Figure 1) and to confirm the amorphous state of a-Li_xTiS_2. The particle size, L_i, after i hours of ball-milling is obtained using the Scherrer equation:

$$L_i = \frac{k\lambda}{\sqrt{W_i^2 - W^2}\cos\Theta} \qquad (1)$$

with W_i and W being the full widths at half-maximum of the most intense diffraction lines of the milled and raw products (particle size ≈ 1 μm), respectively, λ the wavelength (0.1549 nm, Cu Kα), Θ the Bragg angle (in radians), and k a shape factor of typically 0.9. With increasing milling time, the left flank of the diffraction peak becomes increasingly distorted, and a second broad peak emerges at approximately 34°. Decay products of both the hexagonal and the cubic modifications of Li_xTiS_2 as well as alumina from the vial can be excluded as a cause for this additional line, because these do not show reflections near this angle. The diffractograms of the polycrystalline sample and of the material after 1 h of ball-milling (left) were prepared from the same batch, as were the samples subjected to ball-milling for 0.5 and 2 h (right). These preparations allow us to conclude that impurities in the batch cannot be responsible for the second line, because its appearance is clearly dependent on milling time, but not on the batch used. For the estimation of the particle size, the half width of the right side of the peak was used, because it appears to be undistorted. Particle diameters obtained from this procedure are likely to be subject to some systematic error; this, however, should not impose any limitation on the internal comparability of the data. The particle diameter is about 20 nm after only 30 min of ball-milling. Longer milling times (up to 2 h) lead to a further decrease in grain size to about 12 nm (cf. Table 1). Longer milling has no additional effect on the particle size. As expected, the amorphous sample does not show any diffraction peaks.

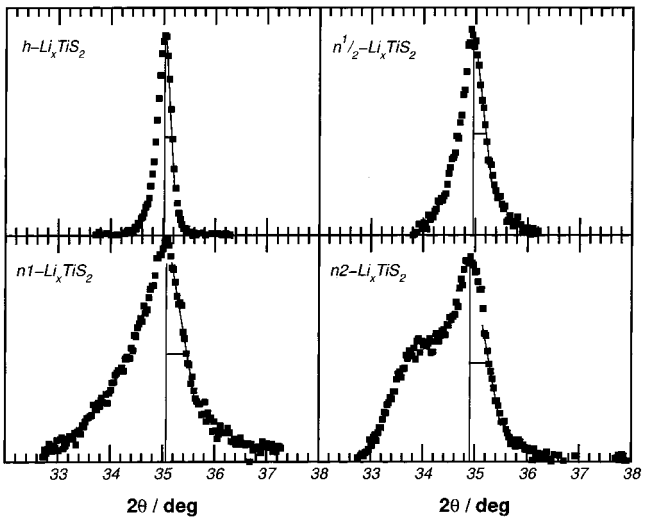

Figure 1. X-ray diffractograms of polycrystalline Li_xTiS_2 and the nanocrystalline material after 0.5, 1, and 2 h of ball-milling. The high-angle flank was used for the particle size estimation. See text for a discussion of the shoulder occurring on the low-angle side.

II. Technique and Setup. ^{7}Li spin−lattice relaxation measurements and NMR spectra were taken using a Bruker MSL 100 console in connection with an Oxford tunable (0−7 T) cryomagnet and a Kalmus LP 400 HF high-frequency amplifier. For most measurements, a commercial Bruker probe was suitable. Temperature was adjusted by means of a stream of tempered air or freshly evaporated nitrogen. For measurements above 550 K, a special home-built high-temperature probe with direct resistance heating[14] was used.

For the spin−lattice relaxation measurements, a saturation−recovery sequence consisting of typically ten 90° saturation pulses, a variable waiting time τ, and another 90° detection pulse was employed. After the last pulse, the free induction decay (FID) in the radio frequency coil was sampled. Pulse durations were of the order of 5 μs. For each data point, that is, each set of temperature and resonance frequency, magnetization was recorded for 30 individual τ times. The measuring time decreased from about 90 min at 140 K to less than 10 min at the highest temperatures.

To reduce the annealing effect that is imposed on the samples because of the high temperature at the time of the measurement, the NMR spectra have been recorded simultaneously with the relaxation data. For this purpose, the most intense FIDs of each data point were added up and then Fourier transformed. This procedure means trading off some signal quality against fast measurement conditions, which protect the samples from getting annealed during the experiment. To make the information from the imaginary part of the spectra accessible, zero filling was applied in the process of Fourier transformation. At the highest frequencies, a field drift during the longer measurements was corrected for by use of a time-dependent phase correction algorithm.[15]

Results

I. Annealing Studies. Because disordered materials are subject to structural rearrangements such as particle growth and phase transformation upon heating, the necessity of a study of

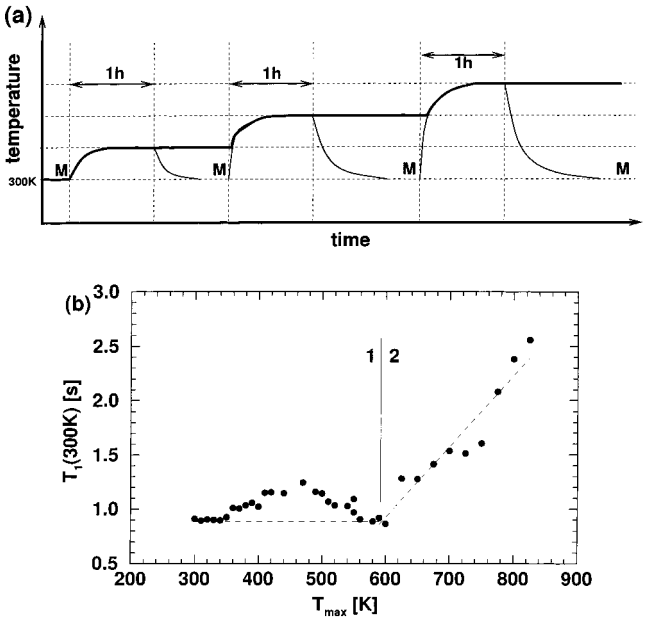

Figure 2. Annealing experiment. (a) Temperature program. Each annealing step is followed by a T_1 measurement ("M") at 300 K. The bold line shows the course of the highest temperature T_{max} to which the sample has been exposed, and the normal line corresponds to the actual temperature. (b) Relaxation time at 300 K vs T_{max}.

the impact of thermal treatment on the samples is obvious. This holds especially for samples prepared by intercalation reactions, because chemical homogeneity needs to be achieved by equilibrating the intercalate concentration.

Both effects of thermal treatment, chemical homogenization (required) and structural relaxation (undesired), were probed using a nanocrystalline sample which had not been homogenized prior to milling. The spin−lattice relaxation rate was measured at 300 K at the beginning of the series and after each 1-h annealing step. During each step, the sample was rapidly heated to a maximum temperature 10 K higher than that reached during the previous step. This means that the heating-up, but not the cooling-down, phases are regarded as part of the annealing time of 1 h. The annealing program and the 300 K relaxation times as a function of the maximum temperature T_{max} to which the sample has been exposed are shown in Figure 2.

From $T_{max} = 340$ K onward, the 300 K relaxation time increases from 0.9 s to 1.3 s at $T_{max} = 470$ K. It then decreases down to its initial value at $T_{max} = 600$ K (regime 1). Beyond this annealing temperature (regime 2), T_1 (300 K) increases linearly with T_{max}.

In regime 1, homogenization of the lithium distribution is achieved. Because of the blocking effect of intercalated lithium ions close to the surface of the host material, a concentration profile is set up within the grains. Upon heating, this profile is flattened. The homogenization process is inhibited during the initial phase, because the lattice has to be stretched along the stacking direction (*c* axis) by the first lithium ions moving in. Therefore, the relaxation time, which at given temperature and NMR frequency is proportional to the mean time an ion stays on its site, increases slightly and then falls back to an equilibrium value. Studies on the intercalation kinetics of layer-structured transition-metal dichalcogenides[16,17] corroborate this concept of the homogenization process. Since this equilibration can be achieved in poly- as well as in nanocrystalline material, all the other samples were homogenized *before* milling.

In regime 2, with monotonically increasing relaxation time, the structural relaxation of the disordered host structure is dominant. In this temperature regime, T_{max} has been incremented in 25 K steps, each lasting for 1 h. We thus assume a linear dependence of T_1 (300 K) on the time the sample is kept above 600 K rather than a linear dependence on T_{max} itself, because the samples are most probably not equilibrated after just 1 h of heating and because the relaxation time of polycrystalline Li_xTiS_2 (8 s under the given conditions) is not reached at the end of the series. Since a typical T_1 measurement takes about 1 h, we have to assume that data taken beyond 600 K are not very reliable. The results presented in this paper are therefore restricted to temperatures below 600 K.

II. Spin−Lattice Relaxation. In Figure 3, an Arrhenian plot, that is, a logarithmic representation of the spin−lattice relaxation rate T_1^{-1} versus inverse temperature, of nanocrystalline Li_xTiS_2 is shown at the resonance frequency $\upsilon_0 = 38.9$ MHz. A typical curve consists of a superposition of a diffusion-induced peak and a weak temperature-dependent background. The flanks of the diffusion-induced peak may be described by an Arrhenian law which reads for the low-temperature side

$$T_{1\,\mathrm{diff}}^{-1} \propto \exp\left(-\frac{E_{\mathrm{nmr}}^{\mathrm{lT}}}{k_{\mathrm{B}}T}\right) \tag{2}$$

with $E_{\mathrm{nmr}}^{\mathrm{lT}}$ being the activation energy and k_B the Boltzmann constant. All activation energies discussed in this section are summarized in Table 1. The background relaxation rate can be described by an empirical power law

$$T_{1\,\mathrm{bgr}}^{-1} \propto T^{\gamma} \tag{3}$$

whose parameter γ is about 1.5, as estimated from the data points at the three lowest temperatures. This value has to be regarded as an upper limit, because the temperature interval used in the calculation comes close to the diffusion-dominated regime. For a detailed analysis of the cause of this background rate, data taken at even lower temperature were required. A contribution due to coupling of the nuclear spin reservoir to conduction electron spins as might be assumed for a semimetal may at best explain a part of the background, because the temperature dependence is predicted to be $\gamma = 1$ in this case, and this phenomenon should be accompanied by a reasonable Knight shift, which has not been observed here. However, subtracting the power law (dashed line in Figure 3) from the measured rate in the entire temperature range leads to pure diffusion-induced residual data. $T_{1\mathrm{diff}}^{-1}$ data points on the left of the vertical line in Figure 3 may be regarded as reliable, that is, the error introduced by the background correction is less than 50% of the actual value. The position and the absolute rate of the diffusion-induced maxima are not significantly altered by the correction procedure; the activation energies found are slightly higher (about 10 meV) than those obtained from the raw data sets (cf. slopes in Figure 3).

An overview of the temperature-dependent spin−lattice relaxation rates of amorphous, nanocrystalline, and polycrystalline Li_xTiS_2 at $\upsilon_0 = 24.5$ MHz is displayed in Figure 4. The rate in polycrystalline Li_xTiS_2[11] shows a marked maximum at 520 K. The activation energy is 0.19 eV. Neither disordered modification shows a well-defined maximum. In the case of the amorphous sample, the peak is very broad, with an activation energy of only 70 meV. The maximum is located at about 400 K. The nanocrystalline sample shows intermediate behavior; the activation energy is 0.16 eV in this case. The rate maximum is not entirely covered, but the decrease in the steepness of the flank indicates that its position is close to the one observed with

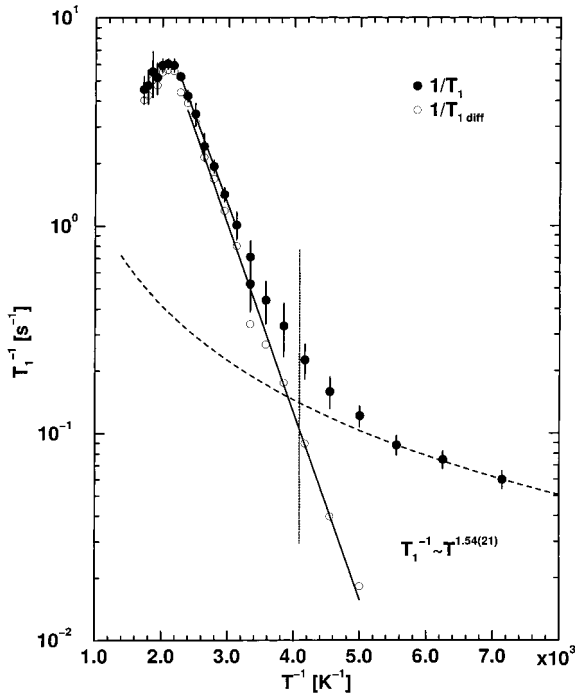

Figure 3. Logarithmic representation of the spin−lattice relaxation rate of nanocrystalline Li_xTiS_2 (after 2 h of milling) vs inverse temperature at $\upsilon_0 = 38.9$ MHz. A power-law temperature dependence (eq 3) is assumed as the background relaxation rate. The background is estimated from the data below 180 K and subtracted from the raw data to reveal the diffusion-induced rate $T_{1\mathrm{diff}}^{-1}$.

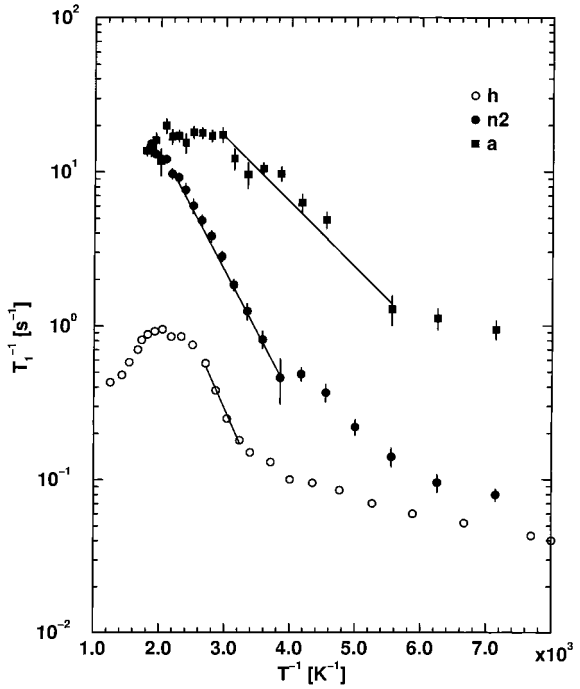

Figure 4. Logarithmic representation of the spin−lattice relaxation rate of amorphous, nanocrystalline, and polycrystalline[11] Li_xTiS_2 vs inverse temperature at $\upsilon_0 = 24.5$ MHz.

the polycrystalline material. This indication is supported by the fact that in one case a maximum was observed (at $\upsilon_0 = 38.9$ MHz) with its position at 500 K. The absolute value of the rate in the diffusion-induced regime is about 1 order of magnitude larger in both disordered forms than in the polycrystalline modification. On the other hand, the background contribution is similar for both crystalline forms, while the background

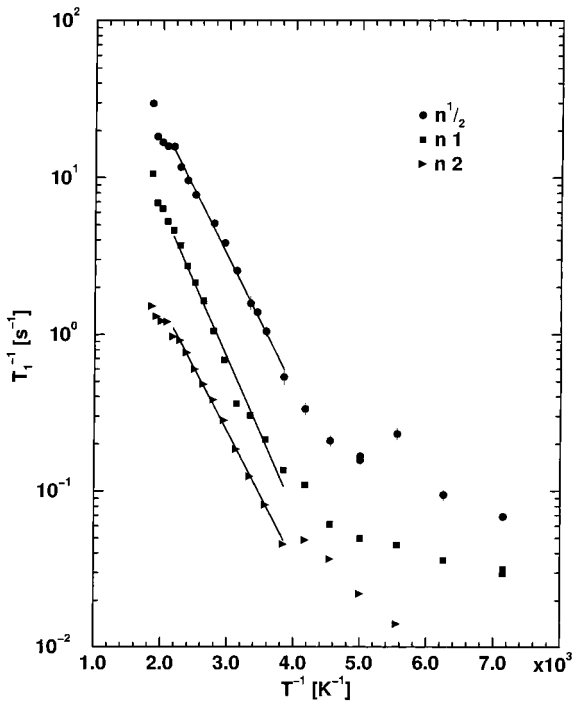

Figure 5. Logarithmic representation of the spin−lattice relaxation rate of nanocrystalline Li_xTiS_2 after different milling times (cf. Table 1) vs inverse temperature at $\upsilon_0 = 24.5$ MHz. The n1 (n2) curves have been shifted down along the ordinate by half a decade (a full decade) for clarity.

relaxation rate of the amorphous material is about 1 order of magnitude higher. Comparing nanocrystalline samples after different milling times (Figure 5), we find no strong differences in the activation energy (0.16−0.19 eV) or in the temperature and rate at the maximum.

Care has to be taken to discriminate pure self-diffusion from ionic motion due to chemical potential gradients in the sample. As described in section III, it is necessary to homogenize the lithium distribution by heating the samples. Because this is not possible in the case of the amorphous material as a consequence of the synthesis technique, the effect of chemical diffusion needs to be estimated. For this purpose, a nonhomogenized nanocrystalline sample was also measured. In Figure 6, Arrhenian plots of amorphous, homogenized, and nonhomogenized nanocrystalline samples are compared (in this plot, only the activation energies, but not the positions of the rate maxima, are comparable, because the measurements are carried out at different frequencies). The nonhomogenized sample clearly has a weaker activation energy (0.12 eV) than the homogenized one (0.16 eV). Nevertheless, it is much higher than $E_{\mathrm{nmr}}^{\mathrm{lT}}$ of the amorphous sample. The influence of structure (nonhomogenized nanocrystalline vs nonhomogenized amorphous material) obviously dominates the effect of chemical diffusion (homogenized vs nonhomogenized material).

The frequency dependence of the relaxation rate (Figure 7) in the temperature regime of the diffusion-induced low-temperature flank can be described by a power law.

$$T_1^{-1} \propto \upsilon_0^{-\beta} \tag{4}$$

Therefore, the regression curves in Figure 7 are limited to the frequency range for which the relaxation rate at 300 K corresponds to the diffusion-induced low-temperature flank. For all disordered modifications, the exponent of the frequency dependence scatters around $\beta = 0.6$; its value is in all cases

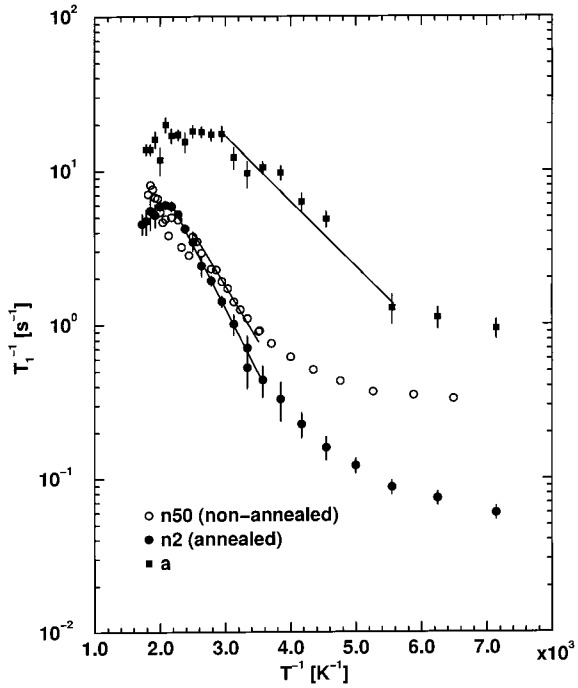

Figure 6. Logarithmic representation of the spin−lattice relaxation rates vs inverse temperature. In contrast to any other nanocrystalline sample, the n50 material was not heat-treated prior to milling.

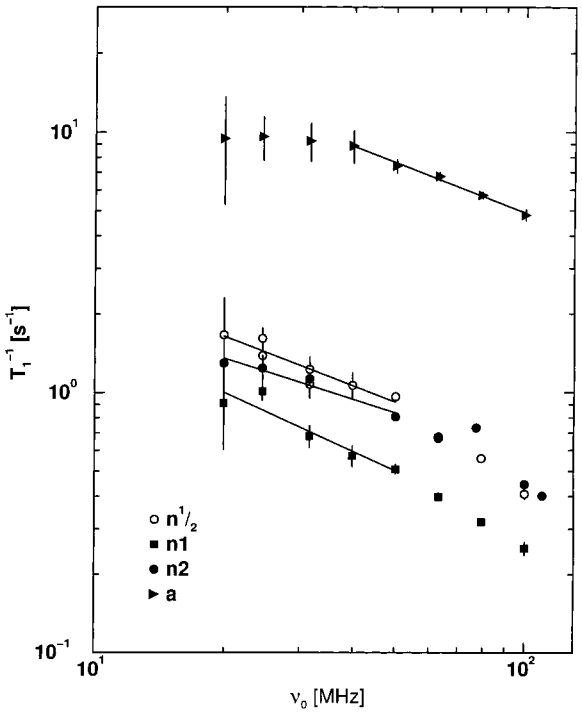

Figure 7. Log−log representation of the spin−lattice relaxation rates of the disordered samples vs resonance frequency at 300 K. Regression lines correspond to the power law eq 4.

significantly below 1. The relaxation of the polycrystalline material is dominated by the background at 300 K; thus, at this temperature the power law (eq 4) is not applicable. In ref 11 an exponent $\beta \approx 1$ was found at 400 K.

III. NMR Spectra. NMR spectra (Figure 8) have been recorded throughout the entire temperature range of the relaxation experiments. For nanocrystalline Li_xTiS_2, a line shape close to the rigid-lattice limit is obtained at the lowest temperatures. In polycrystalline Li_xTiS_2 (Figure 8a), the rigid-lattice situation

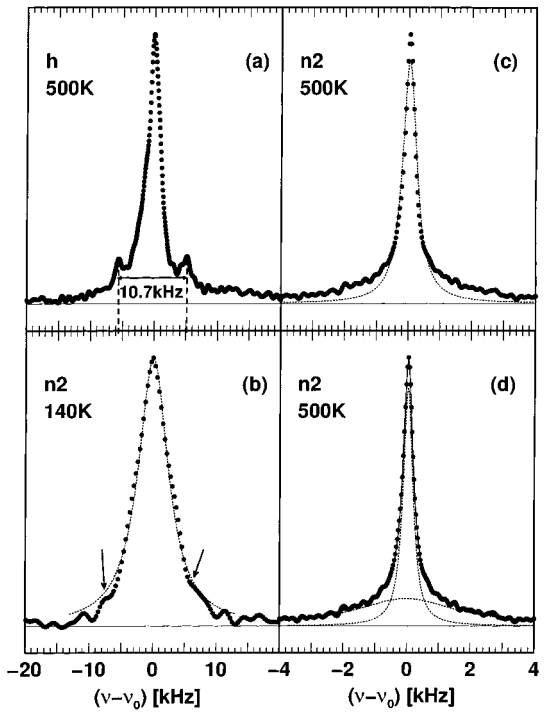

Figure 8. NMR spectra of (a) poly- and (b−d) nanocrystalline Li_xTiS_2 recorded at $\nu_0 = 24.5$ MHz. (a,b) Rigid-lattice conditions. The quadrupole satellites/shoulders are indicated. (c,d) Motionally narrowed spectrum with (c) single- and (d) double-Lorentzian fitted curves. Note the different frequency scales in the left and right columns.

holds even above room temperature. At 500 K, a slightly motionally narrowed central line reveals the quadrupole satellites with a splitting of $\nu_Q = 10.7$ kHz. In a rigid-lattice spectrum of nanocrystalline Li_xTiS_2 (Figure 8b, at 140 K), the satellites are reduced to shoulders with a slightly larger splitting (about 13 kHz) than in the coarser-grained material. In the literature,[18] a value of 12 kHz is reported for polycrystalline material.

At higher temperature, the central line of nanocrystalline Li_xTiS_2 tends to decompose into a narrow and a broad component at the same frequency. Figure 8c shows the inadequacy of a single-Lorentzian line shape function, which is appropriate for the polycrystalline as well as the amorphous forms. A double-Lorentzian shape function agrees perfectly with the data (Figure 8d).

The temperature dependence of the full width at half magnitude (fwhm) of both spectral components is shown in Figure 9a. A single-Lorentzian shape function is appropriate up to 240 K with a constant fwhm of about 6 kHz. In the temperature interval from 260 to 420 K, the decomposition of the line is observed, with a fwhm of about 6 kHz for the broad and less than 1 kHz for the narrow component. At even higher temperature, the broad component starts also to become narrower. The (inadequate) single-Lorentzian fwhm is shown in the figure for comparison. It decreases in the intermediate temperature range where the decomposition effect is observed. This is due to the fact that the relative intensities of both components change with temperature. In particular, the narrow component increases from 0% to about 50% above 350 K (Figure 9b).

Discussion

The interfaces between grains in nanocrystalline materials are described either in terms of wide-angle grain boundaries or as a heavily disordered, maybe amorphous, phase.[19] In an

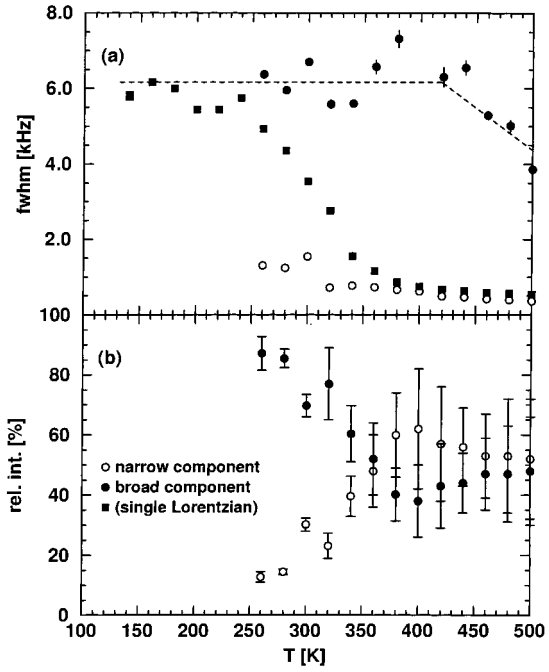

Figure 9. (a) Line widths and (b) relative intensities of the narrow and broad components of the NMR central transitions of nanocrystalline Li_xTiS_2 as a function of temperature. Line widths obtained by an (inadequate) single-Lorentzian fit are displayed for comparison in the top figure.

amorphous structure, the nearest-neighbor distances are distributed around some mean value, leading to a distribution of the heights of the potential energy barriers an ion has to pass when moving through the structure. Ions will obviously tend to preferentially follow pathways along which the barriers to pass are comparatively low. Consequently, the mean barrier height along a diffusion pathway will certainly be smaller in an amorphous structure than in a crystalline structure, even assuming the densities were the same. Taking this into account leads to the notion that the self-diffusion of small ions like lithium should be considerably accelerated in an amorphous structure as a consequence of the distribution of activation barrier heights. Therefore, one recognizes that the diffusion properties of a heterogeneous mixture of crystalline and amorphous phases should be dominated by the amorphous component. This model implies that the activation barriers for diffusing ions in amorphous and nanocrystalline materials are similar and considerably smaller than those in polycrystalline materials. In three-dimensional ion-conducting materials, for example, $LiNbO_3$,[20] the activation energy is in general much lower in the nanocrystalline form. A comparative study of amorphous and nanocrystalline structures in this respect is, to our knowledge, not reported in the literature.

Li_xTiS_2 is, even in the polycrystalline form, a fast ionic conductor with a low activation energy (0.19 eV) because of the wide van der Waals gap between the TiS_2 layers of the host structure. The diffusion takes place two-dimensionally between the layers, as evident from the frequency dependence of T_1^{-1} on the high-temperature flank of the rate maximum.[11] On the other hand, the isotropic amorphous modification shows even lower barriers (70 meV), which implies a barrier height distribution characteristic of glasses in conjunction with the formation of diffusion pathways along which the lowest barriers are located.[21]

If the nanocrystalline material is modeled as an ensemble of crystalline grains in an amorphous matrix, one should expect

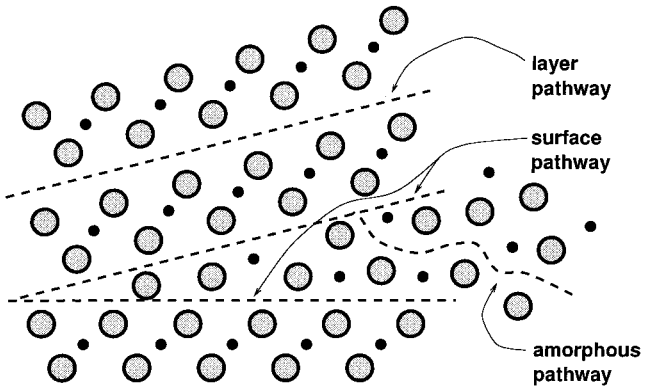

Figure 10. Schematic model of three types of a two-dimensional ionic conductor. Large circles represent anions (sulfur), and small circles lattice cations (titanium). The Li ions are moving along the pathways indicated by dashed lines.

basically amorphous-like barriers and pathway formation. In the present study, we found an activation energy (0.16 eV) that is only slightly reduced as compared to that of the polycrystalline material. This fact may be ascribed to pathway formation on the surface of the nanograins (cf. Figure 10), which provide a kind of guard rail on one side of the pathways. An ion located somewhere in the amorphous matrix phase will sooner or later come along a surface site and then be guided along the surface. A motion in the opposite direction, that is, back from the surface into the amorphous regions, is less likely for statistical reasons, as long as the activation barriers along the surface are low compared to the mean barrier height in the *entire* amorphous phase, which is considerably higher than those 70 meV measured for the mean barrier height *along the pathways* of the amorphous material. If the surface barrier height were larger, the extent of surface trapping would thus be reduced. Eventually, when the surface barrier height is larger than the average barrier height in the amorphous phase, the inverse effect may be expected. This is the usual behavior observed with nanocrystalline three-dimensional ionic conductors if an amorphous intergrain phase is dominating the diffusion. Comparing layered polycrystalline and amorphous samples, it might appear unlikely that the activation energy in the amorphous modification is even lower, because the probability that a moving ion encounters another atom appears to be larger in the disordered structure. However, van der Waals repulsion of sulfide ions will take place in either modification, leading to van der Waals layers or preferred pathways, respectively.

The structural information obtained from the NMR spectra may be used to refine this simple dynamic model. The decomposition of the central transition line into a broad and a narrow component follows from two different types of environment of the probe nuclei. These may be ascribed to ions on bulk and interface sites, respectively. Because the contribution of mobile ions (relative intensity of the motionally narrowed component[7]) depends on the temperature, this would imply a displacement of the grain surface with temperature, which is not plausible as long as grain growth may be excluded (i.e., up to 600 K in this study). On the other hand, the assumption of a gradient structure of the interface may explain the temperature dependence: If those 50% of the ions contributing to the narrow component that is observed in the high-temperature limit are not located on similar amorphous matrix sites but on disordered sites with significantly different local environment depending on the distance from the grain surface, then obviously not all of them start to move freely at the same temperature.

The interface structure proposed here is also capable of explaining the distorted low-angle flank apparent in the X-ray diffractograms of the longer-milled samples (Figure 1). If there is a crystalline region with a heavily distorted lattice surrounding the core grain, and if the average density in this region is slightly lower than inside the grain, then a broad line occurring at a lower angle is the expected pattern from this component. Line shifts originating from lattice distortions in nanocrystalline materials have been reported previously,[22] but in this reference, the core grain itself was distorted, hence an asymmetric broadening was found rather than a separate line.

The frequency dependence of the relaxation rate indicates the disordered structure of the environment of the mobile ions in both amorphous and nanocrystalline Li_xTiS_2. In the temperature regime of the low-temperature flank of the rate maximum, the Bloembergen−Purcell−Pound ("BPP") model[23] for isotropic three-dimensional diffusion predicts $\beta = 2$. The same exponent is also valid for unrestricted two-dimensional jump diffusion.[7,24] Frequency exponents in the regime $1 \leq \beta < 2$ are predicted by several theoretical approaches such as the coupling concept,[25] the jump-relaxation model,[26] and the dynamic structure model.[21] These models assume structural relaxations after a site has been left vacant by a hopping ion, and some also account for Coulomb interactions between the mobile ions, resulting in correlated motion, which is typical of fast ionic conductors.[27,28] Sublinear frequency dependence has been reported for ionic glasses[29,30,31] and is also found in both disordered modifications of Li_xTiS_2 ($\beta \approx 0.6$). A sublinear frequency dependence of the diffusion-induced relaxation rate corresponds to a *super*linear dispersion of the conductivity,[32] which has also been observed in disordered systems.[33] Such an exponent $\beta < 1$ (or its impedance analog) may be interpreted in terms of the unified site relaxation model (USRM),[34] which considers a time-dependent reverse jump probability, adaptation of sites to the presence or absence of a mobile ion, and Coulomb interactions of the charge carriers. Because the USRM is based on the assumption of a flexible, disordered structure rather than a rigid crystal lattice, for an ordered fast ionic conductor (e.g., h-Li_xTiS_2: $\beta \approx 1$) where the structure does not relax after an ion has moved to a neighboring site, one expects $1 \leq \beta < 2$. The deviation from $\beta = 2$ is then caused merely by Coulomb interactions between the fast moving cations.

Conclusions

Li_xTiS_2 is a fast ion conductor, whose hexagonal layered crystal structure facilitates two-dimensional lithium self-diffusion. Besides a polycrystalline reference sample, an amorphous and several nanocrystalline samples were prepared. The lithium content was in all cases about $x = {}^2/_3$.

The annealing behavior of n-Li_xTiS_2 was studied through the dependence of the spin−lattice relaxation time at 300 K on the annealing temperature. An intermediate increase of T_1 (300 K) reveals the necessity of homogenization of the lithium distribution after the intercalation reaction. At annealing temperatures beyond 600 K, T_1 (300 K) increases about linearly with the time the sample is exposed to temperatures higher than 600 K, indicating that structural relaxation takes place.

The spin−lattice relaxation rate T_1^{-1} of ^{7}Li in amorphous, nanocrystalline, and polycrystalline Li_xTiS_2 was measured in the temperature range from 140−600 K and for resonance frequencies from 20−110 MHz. The diffusion-induced rate peaks in an Arrhenian representation are superimposed on a weak power-law background. The activation energies for individual jumps of lithium ions, extracted from the slopes of the low-temperature flanks of the rate peaks, are 190, 160, and 70 meV for h-Li_xTiS_2, n-Li_xTiS_2, and a-Li_xTiS_2, respectively. The frequency dependence of T_1^{-1} follows a power law with an exponent $\beta \approx 0.6$ for both disordered modifications and $\beta \approx 1$ for h-Li_xTiS_2.

NMR spectra were calculated from the relaxation data by Fourier transformation. The line shapes of the spectra change from rigid-lattice to motionally narrowed type upon increasing temperature. Rigid-lattice spectra of h-Li_xTiS_2 consist of a central line and quadrupole satellites; in the case of n-Li_xTiS_2, these are visible only in the form of shoulders. The a-Li_xTiS_2 spectra are slightly motionally narrowed even at 140 K. Contrary to those of the polycrystalline and amorphous forms, the central lines of n-Li_xTiS_2 decompose into a broad and a narrow component during the process of motional narrowing. The relative intensity of the narrow component increases with temperature, reaching 50% in the high-temperature limit.

A schematic model for the diffusion process in two-dimensional fast ion-conducting nanocrystalline materials is proposed on the basis of the above dynamical and structural results. We conclude that the interfacial regions are inhomogeneous and the lithium ions are confined to the surface of the nanograins if the activation energy along surface diffusion pathways is small compared to the average barrier height of the heavily disordered intergranular material.

Acknowledgment. We would like to thank Dr. Roderich Röttger for assistance with the X-ray diffractometer, which belongs to the group of Prof. Hermann Schmalzried at this institute. Discussion with and technical assistance of Dr. Gerd Balzer, Institut für Anorganische Chemie, Universität Hannover, are gratefully acknowledged. Part of this work was funded by the Deutsche Forschungsgemeinschaft (Sonderforschungsbereich 173). P.H. would also like to acknowledge financial help by the Fonds der Chemischen Industrie.

References and Notes

(1) Whittingham, M. S. *Prog. Solid State Chem.* **1978**, *12*, 41.
(2) *Proceedings of the NATO Advanced Research Workshop on New Promising Electrochemical Systems for Rechargeable Batteries*; Barsukov, V., Ed.; Kluwer: Dordrecht, 1996.
(3) Croce, F.; Passerini, S.; Scrosati, B. *J. Electrochem. Soc.* **1994**, *141*, 1405.
(4) Plichta, J.; Behl, W. K.; Chang, W. H. S.; Schleich, D. M. *J. Electrochem. Soc.* **1994**, *141*, 1418.
(5) Ngai, K. L. *J. Non-Cryst. Solids* **1996**, *203*, 232.
(6) Angell, C. A. *Annu. Rev. Phys. Chem.* **1992**, *43*, 693.
(7) Heitjans, P.; Schirmer, A. In *Diffusion in Condensed Matter*; Kärger, J., Heitjans, P., Haberlandt, R., Eds.; Vieweg: Braunschweig, Springer: Berlin, 1998; p 116.
(8) Gleiter, H. *Phys. Status Solidi B* **1992**, *172*, 41.
(9) Whittingham, M. S. *J. Electrochem. Soc.* **1976**, *123*, 315.
(10) Umrigar, C.; Ellis, D. E.; Wang, D.; Krakauer, H.; Posternak, M. *Phys. Rev. B* **1982**, *26*, 4935.
(11) Küchler, W.; Heitjans, P.; Payer, A.; Schöllhorn, R. *Solid State Ionics* **1994**, *70*, 434.
(12) Bensalem, A.; Schleich, D. M. *Mater. Res. Bull.* **1988**, *23*, 857.
(13) Dines, M. B. *Mater. Res. Bull.* **1975**, *10*, 287.
(14) Franke, W. Ph.D. Thesis, Universität Hannover, 1993; p 33.
(15) Winter, R. Ph.D. Thesis, Universität Hannover, 1998; p 56.
(16) Wang, J. C. *Solid State Ionics* **1990**, *40*, 548.
(17) Ramos, C.; Lerf, A.; Butz, T. *Ber. Bunsen-Ges. Phys. Chem.* **1989**, *93*, 1209.
(18) Silbernagel, B. G.; Whittingham, M. S. *J. Chem. Phys.* **1976**, *64*, 3670.
(19) Siegel, R. W. *Encycl. Appl. Phys.* **1994**, *11*, 173.
(20) Bork, D.; Heitjans, P. *J. Phys. Chem. B* **1998**, *102*, 7303.
(21) Bunde, A.; Maass, P. *Physica A* **1993**, *200*, 80.
(22) Beck, Ch.; Bruch, Ch.; Ehses, K.-H.; Hempelmann, R. *J. Phys. IV* **2000**, *10*, Pr7−87.

(23) Bloembergen, N.; Purcell, E. M.; Pound, R. V. *Phys. Rev.* **1948**, *73*, 679.
(24) Bjorkstam, J. L.; Villa, M. *Magn. Reson. Rev.* **1980**, *6*, 1.
(25) Ngai, K. L.; Kanert, O. *Solid State Ionics* **1992**, *53*, 936.
(26) Funke, K. *Prog. Solid State Chem.* **1993**, *22*, 111.
(27) Meyer, M.; Maass, P.; Bunde, A. *Phys. Rev. Lett.* **1993**, *71*, 573.
(28) Bunde, A.; Maass, P.; Meyer, M. In *Diffusion in Condensed Matter*; Kärger, J., Heitjans, P., Haberlandt, R., Eds.; Vieweg: Braunschweig, Springer: Berlin, 1998; p 319.
(29) Franke, W.; Heitjans, P. *Ber. Bunsen-Ges. Phys. Chem.* **1992**, *96*, 1674.
(30) Winter, R.; Siegmund, K.; Heitjans, P. *J. Non-Cryst. Solids* **1997**, *212*, 215.
(31) Balzer-Jöllenbeck, G.; Kanert, O.; Jain, H.; Ngai, K. L. *Phys. Rev. B* **1989**, *39*, 6071.
(32) Meyer, M.; Maass, P.; Bunde, A. *J. Non-Cryst. Solids* **1994**, *172*−*174*, 1292.
(33) Pradel, A.; Taillades, G.; Cramer, C.; Ribes, M. *Solid State Ionics* **1998**, *105*, 139.
(34) Bunde, A.; Funke, K.; Ingram, M. D. *Solid State Ionics* **1996**, *86*−*88*, 1311.